

Learning to Boost Filamentary Structure Segmentation

Lin Gu

Bioinformatics Institute (BII)

Agency for Science Technology and Research

(A*STAR)

Email: gulin@bii.a-star.edu.sg

Li Cheng

Bioinformatics Institute (BII)

Agency for Science Technology and Research

(A*STAR)

Email: chengli@bii.a-star.edu.sg

Abstract—The challenging problem of filamentary structure segmentation has a broad range of applications in biological and medical fields. A critical yet challenging issue remains on how to detect and restore the small filamentary fragments from backgrounds: The small fragments are of diverse shapes and appearances, meanwhile the backgrounds could be cluttered and ambiguous. Focusing on this issue, this paper proposes an iterative two-step learning-based approach. Our approach is rather generic and can be easily augmented to a wide range of existing supervised/unsupervised segmenters to produce an improved result. This has been empirically verified on three specific filamentary structure segmentation tasks including as 2D and 3D neuronal segmentations, where noticeable improvement has been shown over the original state-of-the-arts.

I. INTRODUCTION AND OUR APPROACH

This work aims to address the problem of image-based filamentary structure segmentation in 2D or 3D. In particular, we focus on the challenging issue of preserving weak foreground signals, i.e., small and thin filaments from ambiguous backgrounds. This problem is fundamental in a rather broad range of applications including neuronal tracing from microscopic images [10]. Difficulties of this problem lie in the high variability of filament shape, texture and thickness, which is further complicated by the often noisy and cluttered background that at times could even confuse a trained eye [1].

Existing methods can be roughly categorized into three types: Hessian-based, model-based and learning-based. Hessian-based models make use of the second order derivatives either to guide the development of snake [17], to detect filament edges [2], or to combine with the eigenvalues [7] for segmenting filamentary structures. They however often lack the flexibility to tackle irregular filamentary structures. Model-based methods instead emphasize on fitting filaments with known geometric shapes [8], [19], [16]. Learning-based methods [13], [12], [15], [6], on the other hand, advocate the automation of the feature learning process.

In addition to the binary segmentation result, many of the aforementioned methods also produce a pixelwise *confidence map*, despite the heterogeneous nature of these methods. A confidence map is a spatial mapping with each image pixel assigned a non-negative score, which is larger if this pixel more likely belongs to the filamentary structure foreground, or lower if the other way around. This concept has in fact been adopted by existing methods under different names, such as vesselness [7] and turbularity score [16], [15]. It has been

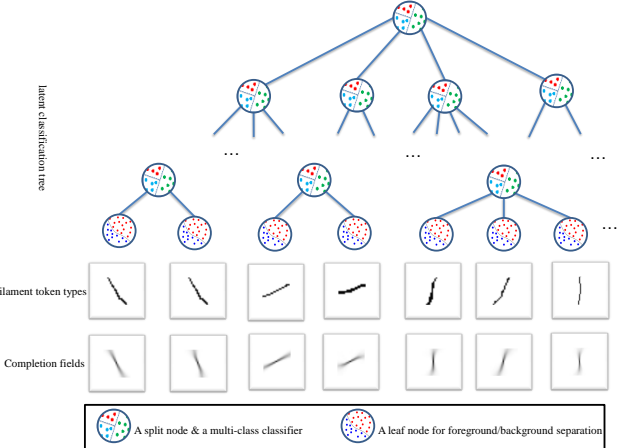


Fig. 1: An illustration of the latent classification tree (LCT) model in step one: A latent split node which comprises a subset of similar tokens and is split into multi-branches according to a multi-class classifier; A leaf node corresponds to a local foreground/background separation problem, with the set of foreground filaments precisely corresponding to a unique token type, as displayed in the second row. For each token type, its completion field is presented in the third row. In the legend: a split node contains a multi-class classifier, while a leaf node has its local foreground/background separation problem.

observed that state-of-the-art methods usually work well on the long & thick filaments, therefore, placing a sufficiently high threshold on the confidence map would produce solely true positive foreground comprising of the main trunk. The observations inspire us to propose a data-driven learning approach aiming at boosting the existing methods' performance on the low confidence region, where our approach specifically focuses on detecting and restoring small foreground filaments from ambiguous backgrounds, a bottleneck issue of many state-of-the-art methods.

To achieve this, an iterative two-step learning-based approach is proposed to boost the performance based on a base segmenter arbitrarily chosen from a number of existing segmenters:

Preprocessing: Obtain the partial segmentation by placing a sufficiently high threshold τ_h on the confidence map. Define a scanning horizon as epsilon ball B with a searching radius ϵ centered around current partial segmentation in the image space.

Step One: In the remaining low confidence regions within the scanning horizon B , detect the filamentary fragments from backgrounds in those pixels with weak confidence in the range of (τ_l, τ_h) . This is achieved by a latent classification tree model. The latent classification tree (LCT) model, as shown in Fig.1, is learned based on a large number of distinct local foreground/background separation scenarios, which are geometrically organized into a tree structure. This divide-and-conquer strategy not only reduces the complexity of the original problem but also introduces specific completion fields encoding the reconstruction guidance. Following the idea of sketch tokens [9], we identify the separation scenario in Fig by grouping similar filamentary fragments in terms of their orientations, shapes and textures as illustrated in Fig.1. The detected filamentary fragments are on the other hand usually isolated from the main trunk due to missing edges. **Step Two:** Grow current filamentary structure by restoring the detected filamentary fragments, i.e., connecting them back to the main trunk. This is achieved by making novel usage of the matting technique guided with the completion fields of these filamentary fragments, as in Fig.2.

Progress Check: Update the scanning horizon by increasing the searching radius ϵ . Go back to step one if the image space has not been entirely explored, otherwise terminate.

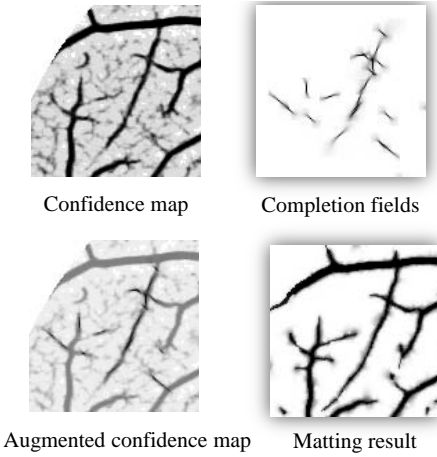


Fig. 2: An example of restoring the missing connections between the detected filamentary fragments and main trunk using the matting technique.

II. EXPERIMENTS

A modified F1 measure to allow minor location offsets similar to [5], [14] is used as follows: When a segmented object is not exactly matched to the ground-truth annotation, it will give a miss as well as a false alarm. In light of this, we assign each miss pixel the distance of its nearest false alarm pixel. If there is a nearest false alarm within deviation range r , the miss pixel is still regarded as a true positive. The precision is thus computed as $\frac{tp}{t}$ where tp is the number of true positive pixels and the t is the total number of positive pixel. In our experiments, the deviation range is set to $r = 1.5$ for 2D applications and $r = 1.8$ for 3D applications. Following [14], the recall is computed based on the centreline of the true positive and ground-truth image. The modified F1 measure is then defined as the harmonic

TABLE I: Performance on 2D Neuronal dataset with different base methods using modified F1 measure.

	Kernel Boost [6]	OOF [8]	Eigen [7]	T2T [3]
Base	84.74	63.50	63.94	66.49
Ours	86.80	66.03	66.85	66.91
% gain	2.06	2.53	2.91	0.42

mean of the precision and recall. In all the experiments, the best such F1 score is reported. In addition, for 3D neuronal datasets we evaluate the metric of averaged absolute centerline deviation (AACD) as follows. Let \mathcal{P} and \mathcal{G} denote the sets of predicted and ground-truth foreground pixels, respectively. Denote a foreground pixel $x_p \in \mathcal{P}$ and similarly a background pixel $x_g \in \mathcal{G}$. Define $d(x_p, x_g)$ the 3D Euclidean distance between these two pixels. The AACD metric between the predicted and the ground-truth segmentation is defined by $\text{AACD}(\mathcal{P}, \mathcal{G}) = \text{avg}\left(\min_{x_p \in \mathcal{P}, x_g \in \mathcal{G}} (d(x_p, x_g))\right)$, where avg is an average operator.

Table I shows that on average our approach produces around 2% performance gain in term of the modified F1 measure. Similar to 2D retinal datasets, our approach is able to boost the performance over different base methods ranging from unsupervised [8], [7] to supervised such as [6], [3]. This is also observed in the follow-up experiments to be described during 3D neuronal segmentation. Visually our result is often noticeably better than that of existing methods, as exemplified in Fig. 3.

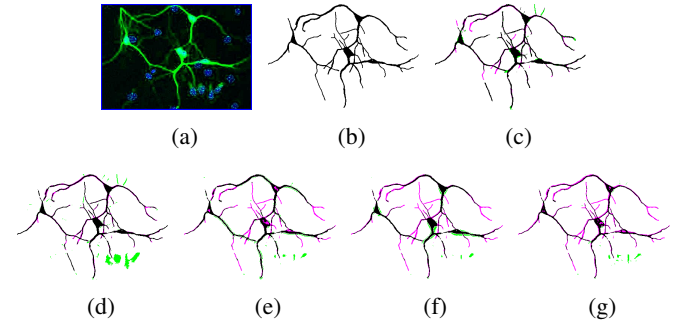


Fig. 3: Performance of 2D neuronal dataset. (a) Input image where the contrast has been increased for visual presentation. (b) Ground-truth annotation. (c) Our method based on [6]. (d) Kernel Boost [6]. (e) OOF [8]. (f) Eigen [7]. (g) T2T [3]. True positive is denoted in black, false positive in cyan and false negative in green.

Experiments are also conducted on the 3D neuronal data including the Olfactory Projection Fibers (OPF) in DIADEM challenge [?] and some samples in BigNeuron Project [11]¹. The base methods are OOF [8], Eigen [7], LEFD [4], Multiscale Enhancement [20] and the gray-weighted distance transform (GWDT) used in APP2 [18]. We quantitatively evaluate our method on the OPF dataset which provides the groundtruth. As presented in Table II when using the modified F1 measure, our method achieves a performance boost of 2 – 5% over all of existing methods depending on the base method’s performance. Moreover, a close examination of the amount of centerline deviation using the AACD metric as

¹<http://bigneuron.org>

TABLE II: Performance on 3D Neuronal OPF dataset with different base methods using modified F1 measure.

	OOF [8]	Eigen [7]	LEFD [4]	mE [20]	GWDT [18]
Base method	49.17	52.27	54.50	62.17	66.83
Our method	53.26	57.27	58.56	64.73	68.39
gain %	4.09	5.00	4.06	2.56	1.56

TABLE III: Performance on 3D neuronal OPF dataset with different base methods using AACD metric (in pixel unit).

	OOF [8]	Eigen [7]	LEFD [4]	mE [20]	GWDT [18]
Base method	3.4162	6.4849	2.5055	1.6977	1.1638
Our method	1.7860	1.7352	1.5915	1.6161	1.1561

described in Table III reveals that our approach dramatically reduce the deviation over the base methods. Fig. 4 demonstrates that visually our result is closer to the ground-truth than the comparison methods.

We also illustrate the utility of neuron tracking on some samples in BigNeuron Project [11]. As illustrated in Fig 5, our method manges to track the tiny filaments which seem to be broken from the main branch.

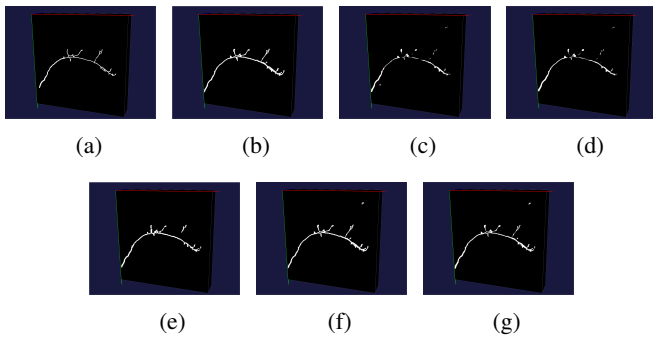


Fig. 4: Performance on 3D Neuronal OPF dataset. (a) Groundtruth annotation (b) Our method based on [20], (c) OOF [8],(d) Eigen [7]. (e) LEFD [4]. (f) multiScaleEnhancement [20]. (g) GWDT: [18].

III. CONCLUSION AND OUTLOOK

To address the problem of image-based filamentary structure segmentation, we propose a value-added approach to improve over a broad set of existing segmenters, with an emphasis on addressing the challenging aspect of preserving small and thin filaments from ambiguous backgrounds. This is achieve by a learning based iterative pipeline that start from an initial partial segmentation, to detect filamentary fragments with a novel LCT model and to restore them back to the current partial segmentation and repeat until there is no change in the segmentation result. Our approach is empirically demonstrated to be capable of improving over a number of existing methods on very different applications. For future work, we plan to evaluate on new biomedical applications such as digital subtraction angiography and magnetic resonance angiography.

REFERENCES

- [1] M. Abramoff, M. Niemeijer, M. Viergever, and B. Ginneken. Ridge based vessel segmentation in color images of the retina. *IEEE Trans. Med. Imag.*, 23(4):501–509, 2004. 1
- [2] P. Bankhead, C. Scholfield, J. McGeown, and T. Curtis. Fast retinal vessel detection and measurement using wavelets and edge location refinement. *PLoS ONE*, 2012. 1
- [3] S. Basu, A. Aksel, B. Condron, and S. Acton. Tree2tree: Neuron segmentation for generation of neuronal morphology. In *ISBI*, 2010. 2
- [4] S. Basu, C. Liu, and G. Rohde. Localizing and extracting filament distributions from microscopy images. *Journal of Microscopy*, 258(1):13–23, 2015. 2, 3
- [5] C. Becker, K. Ali, G. Knott, and P. Fua. Learning context cues for synapse segmentation. *IEEE Trans. Med. Imag.*, 32(10):1864–77, 2013. 2
- [6] C. Becker, R. Rigamonti, V. Lepetit, and P. Fua. Supervised feature learning for curvilinear structure segmentation. In *MICCAI*, 2013. 1, 2
- [7] A. Frangi, W. Niessen, K. Vincken, and M. Viergever. Multiscale vessel enhancement filtering. In *MICCAI*. 1998. 1, 2, 3
- [8] M. Law and A. Chung. Three dimensional curvilinear structure detection using optimally oriented flux. In *ECCV*. 2008. 1, 2, 3
- [9] J. Lim, C. Zitnick, and P. Dollar. Sketch tokens: A learned mid-level representation for contour and object detection. In *CVPR*, 2013. 2
- [10] E. Meijering. Neuron tracing in perspective. *Cytometry A*, 77(7):693–704, 2010. 1
- [11] H. Peng, E. Meijering, and G. Ascoli. From diadem to bigneuron. pages 1–2, 2015. 2, 3
- [12] R. Rigamonti and V. Lepetit. accurate and efficient linear structure segmentation by leveraging ad hoc features. In *MICCAI*, 2012. 1
- [13] J. Soares, J. Leandro, R. Cesar, H. Jelinek, and M. Cree. Retinal vessel segmentation using the 2-d gabor wavelet and supervised classification. *IEEE Trans. Med. Imag.*, 25(9):1214–22, 2006. 1
- [14] E. Turetken, C. Becker, P. Glowacki, F. Benmansour, and P. Fua. Detecting irregular curvilinear structures in gray scale and color imagery using multi-directional oriented flux. In *ICCV*, 2013. 2
- [15] E. Turetken, F. Benmansour, B. Andres, H. Pfister, and P. Fua. Reconstructing loopy curvilinear structures using integer programming. In *CVPR*, 2014. 1
- [16] E. Turetken, G. Gonzalez, C. Blum, and P. Fua. Automated reconstruction of dendritic and axonal trees by global optimization with geometric priors. *Neuroinformatics*, 9(2-3):279–302, 2011. 1
- [17] Y. Wang, A. Narayanaswamy, C. Tsai, and B. Roysam. A broadly applicable 3-d neuron tracing method based on open-curve snake. *Neuroinformatics*, 9(2-3):193–217, 2011. 1
- [18] H. Xiao and H. Peng. App2: automatic tracing of 3d neuron morphology based on hierarchical pruning of a gray-weighted image distance-tree. volume 29, pages 1448–54, 2013. 2, 3, 4
- [19] T. Zhao, J. Xie, F. Amat, N. Clack, P. Ahammad, H. Peng, F. Long, and E. Myers. Automated reconstruction of neuronal morphology based on local geometrical and global structural models. *Neuroinformatics*, 9(2-3):247–261, 2011. 1
- [20] Z. Zhou, S. Sorensen, H. Zeng, M. Hawrylycz, and H. Peng. Adaptive image enhancement for tracing 3d morphologies of neurons and brain vasculatures. volume 13, pages 153–66, 2015. 2, 3, 4

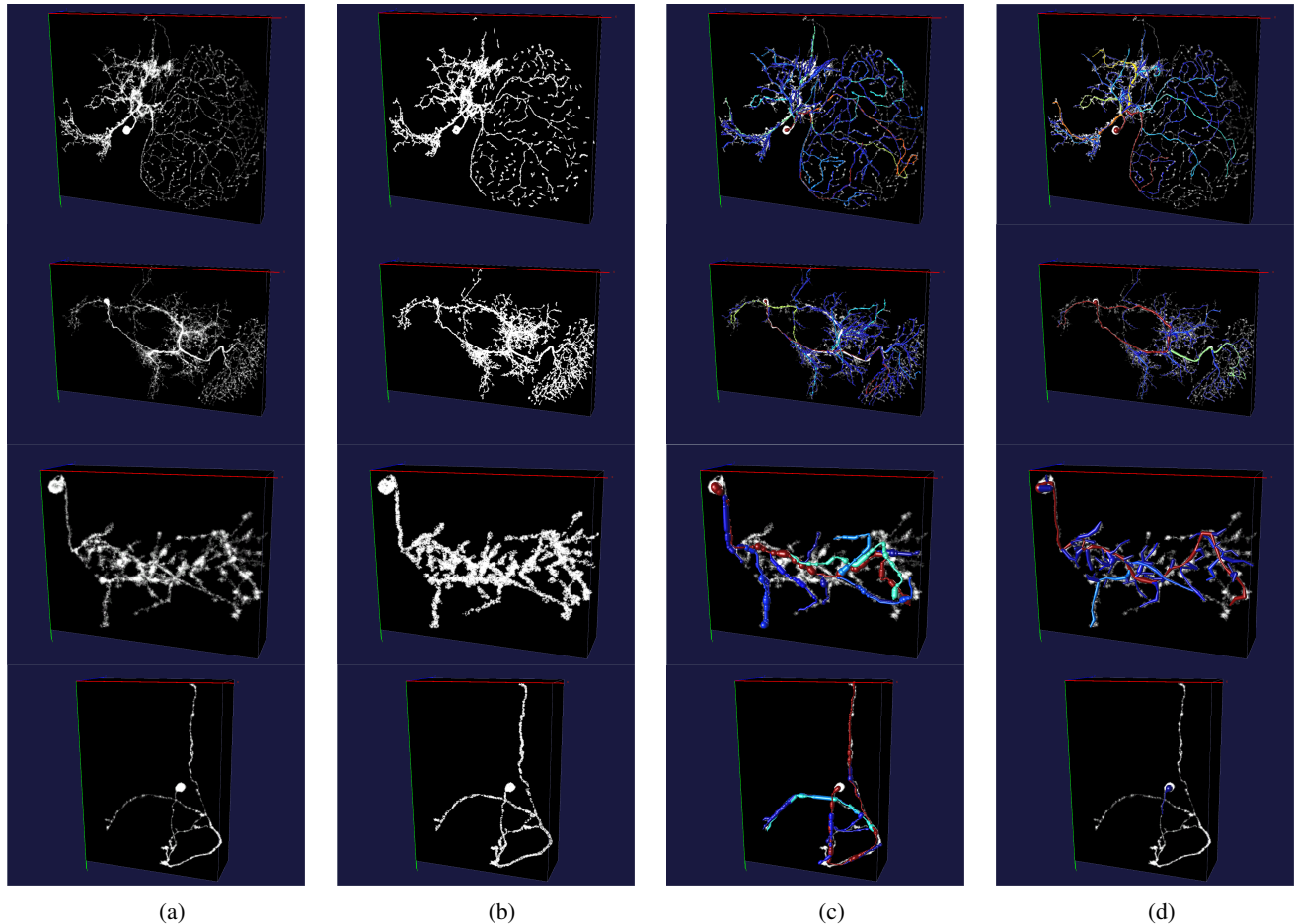


Fig. 5: Tracing performance on BigNeuron dataset. (a) Input image where the contrast has been increased for visual presentation. (b) The partial segmentation based on [20]. (c) Our tracing result based on [20]. (d) Tracing result of APP2 [18].